Journal of Molecular Graphics and Modelling 27 (2008) 342–348

Contents lists available at ScienceDirect

Journal of Molecular Graphics and Modelling

journal homepage: www.elsevier.com/locate/JMGM

How amantadine and rimantadine inhibit proton transport in the M2 protein channel

Pathumwadee Intharathep [a], Chittima Laohpongspaisan [a], Thanyada Rungrotmongkol [a], Arthorn Loisruangsin [b], Maturos Malaisree [a], Panita Decha [a], Ornjira Aruksakunwong [c], Krit Chuenpennit [a], Nopphorn Kaiyawet [a], Pornthep Sompornpisut [a], Somsak Pianwanit [a], Supot Hannongbua [a,*]

[a] Department of Chemistry, Faculty of Science, Chulalongkorn University, Phayathai Road, Patumwan, Bangkok 10330, Thailand
[b] Faculty of Liberal Arts and Science, Kasetsart University Kamphaeng Saen Campus, Nakorn Pathom 73140, Thailand
[c] Department of Chemistry, Faculty of Science, Rangsit University, Pathumtani 12000, Thailand

ARTICLE INFO

Article history:
Received 29 February 2008
Received in revised form 25 May 2008
Accepted 2 June 2008
Available online 8 June 2008

Keywords:
Influenza A
M2 channel
Amantadine
Rimantadine
Molecular dynamics simulations

ABSTRACT

To understand how antiviral drugs inhibit the replication of influenza A virus via the M2 ion channel, molecular dynamics simulations have been applied to the six possible protonation states of the M2 ion channel in free form and its complexes with two commercial drugs in a fully hydrated lipid bilayer. Among the six different states of free M2 tetramer, water density was present in the pore of the systems with mono-protonated, di-protonated at adjacent position, tri-protonated and tetra-protonated systems. In the presence of inhibitor, water density in the channel was considerably better reduced by rimantadine than amantadine, agreed well with the experimental IC_{50} values. With the preferential position and orientation of the two drugs in all states, two mechanisms of action, where the drug binds to the opening pore and the histidine gate, were clearly explained, *i.e.*, (i) inhibitor was detected to localize slightly closer to the histidine gate and can facilitate the orientation of His37 imidazole rings to lie in the close conformation and (ii) inhibitor acts as a blocker, binding at almost above the opening pore and interacts slightly with the three pore-lining residues, Leu26, Ala30 and Ser31. Here, the inhibitors were found to bind very weakly to the channel due to their allosteric hindrance while theirs side chains were strongly solvated.

1. Introduction

In recent years, pandemics of influenza virus A subtype H5N1 have caused more fatalities in humans and animals worldwide, resulting in temporary debilitation, with significant economic consequences [1–3]. An important and growing problem of resistance to anti-influenza virus drugs calls for the need to eventually develop more effective therapies for this viral subtype. The main goal of this study is to understand known drug-target interactions as well as related properties at the molecular level, which is the key to success in designing and discovering new and more potent inhibitors.

The surface membrane proteins of the influenza virus A consist of three important components, hemagglutinin, neuraminidase, and M2 channels [4]. The M2 channel is a homotetrameric protein consisting of 97 residues per subunit. Each subunit comprises an extracellular N-terminal domain (24 residues), a transmembrane (TM) domain (19 residues), and an intracellular C-terminal domain (54 residues) [5–7]. The viral M2 protein functions as a proton selective channel which is activated by low pH environments as found in endosomes [8]. The main functional machinery of the proton-selective M2 channel is believed to lie within the TM helical bundle that exhibits proton conductive activity [9]. In the TM region, the ionizable His37 acts as a proton selectivity with the indole side chain of Trp41 acts as a proton gate to occlude the pore. A structural information for M2-TM has been achieved by Fourier transform infrared spectroscopy [10], solid-state NMR spectroscopy [11–13], UV resonance Raman spectroscopy [14], electron spin resonance [15], cysteine mutagenesis [16], and molecular dynamics simulations [17].

Based on a tetrameric channel, the protonation on histidine tetrad has been identified into different possible states [18]. In

* Corresponding author. Tel.: +66 22 187602; fax: +66 22 187603.
E-mail address: supot.h@chula.ac.th (S. Hannongbua).

1093-3263/$ – see front matter © 2008 Elsevier Inc. All rights reserved.
doi:10.1016/j.jmgm.2008.06.002

terms of pH estimations, the M2 channel shows pH > 7 for the two states with neutral histidine (0H) and histidine dimer (2Hd), representing the closed channel state. Conversely, the acid activation at pH < 7, such as tri-protonated (3H) and fully-protonated (4H) histidine tetrad, reveal the opening form feature. These are suggested by the ^{15}N NMR spectra [19].

Accordingly, two hypothetical mechanisms, proton shuttling [16] and swinging door [20], have been proposed for the M2 proton conduction. In shuttling mechanism, one of the His37 tetrad is necessarily protonated in which an imidazole nitrogen atom is firstly protonated and then another nitrogen atom at the same His37 releases its proton to the interior of the virus. For the swinging mechanism, protons can pass through the water-filled channel due to the electrostatic repulsion between positively charged histidine imidazole rings.

Amantadine (1-aminoadamantane hydrochloride) and rimantadine (α-mehyl-1-adamantane methylamine hydrochloride), an amantadine analogue, are commercial drugs (Fig. 1c) used for the prophylaxis and treatment of influenza A [21,22] by inhibiting the ion-channel activity of the M2 protein [23–26]. However, the mechanism of how they interact with the M2 protein is still controversial. Conventionally, a hypothesis of inhibition invokes interactions of the drug with the mount of the M2 pore, in which the inhibitor behaves as a 'blocker' [25,27,28]. In this view, the adamantyl group interacts with Val24 and Ala27 via van der Waals interactions, while the charged amine group hydrogen bonds with Ser31. Alternatively, Pinto and co-workers [16,29] proposed another model: that amantadine binds to a location deeper in the channel and its ammonium group hydrogen bonds with the His37 side chain. Binding of the drug is supposed to block proton channel activity by displacing water molecules that are essential for proton conduction. It may act as an allosteric inhibitor binding outside the pore region, which consequently leads to the conformation changes of the channel from the open state to closed state [30,31]. ^{1}H NMR spectroscopy data showed that amantadine interacts weakly with the liposomes, suggesting a mechanism by which it may first bind to the lipid bilayers and then block target channels after diffusion across the membrane surface [32]. Recently, ^{15}N CPMAS NMR spectroscopy was used to study the effect of amantadine binding to the His37 side chain as a function of pH, implying a mechanism whereby amantadine interferes with the histidine facilitation of proton conductance [33]. In addition, the MS-EVB simulation indicated that the triply protonated His37 state is the most likely open state with the estimated pH value of 5.5 and amantadine can reduce the proton conductance by 99.8% where its primary binding site to the M2 channel is Ala29 [34].

The controversial question above, how drugs inhibit the M2 proton channel, is the ultimate goal of this study. Thus, molecular dynamics simulations in a fully hydrated lipid bilayer were carried out, starting from the experimentally determined NMR structures of the M2 protein with six possible histidine gate protonation states and their complexes with two inhibitors. The results were monitored in terms of inhibitor–solvent and inhibitor–protein interactions, aiming to understand characteristics of the inhibitors in preventing proton transport through the M2 channel.

2. Computational methods

2.1. Initial structure of the M2 helix bundle and its complexes

The NMR structures of the M2 channel without and with amantadine taken from the Protein Data Bank [PDB entry codes: 1NYJ [12] and 2H95 [33]] were used for the initial M2 helix bundle for the free enzyme and two M2-inhibitor complexes, respectively. The amantadine coordinates are unavailable in the PDB structures [33]; therefore, molecular docking was then applied using the program Autodock 3.0 [35] to generate an initial structures of both M2-amantadine and M2-rimantadine complexes for MD simulations.

2.2. Molecular dynamics simulations

Due to the lack of experimental data on the protonation state (PS) of the histidine residue of the tetra-M2 helix bundle, the simulated systems were constructed for six possible states of the four histidine residues, namely, non-PS (0H), single PS (1H), double PS at adjacent (2Ha) and diagonal (2Hd) positions, triple PS (3H), and quadruple PS (4H). Therefore, eighteen different simulations, six of free forms and twelve of complexes with amantadine and rimantadine, were taken into consideration.

Each system was separately built according to the designed protonation state of the M2 channel with/without inhibitor as described above and then was inserted into a pre-equilibrated lipid bilayer, initially made up of 80 molecules of 1-palmitoyl-2-oleoyl-sn-glycerol-3-phosphatidylcholine (POPC) lipid [36] embedded in

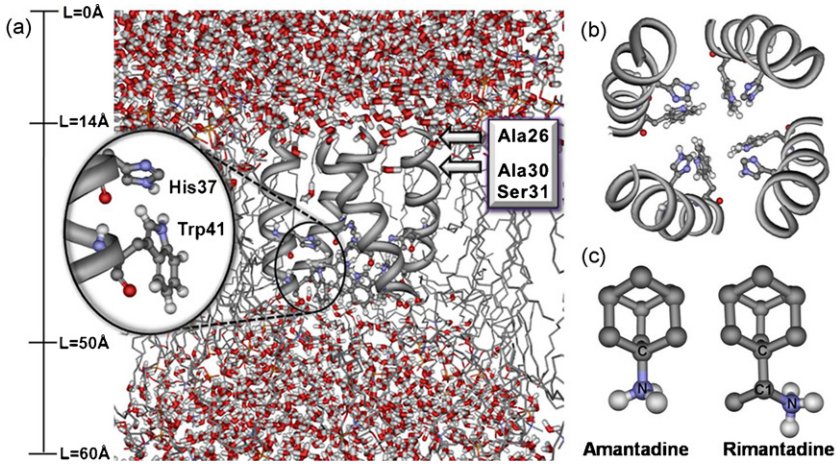

Fig. 1. Schematic of M2 channel and its inhibitors. (a) Side view of the M2 channel with Leu26, Ala30, Ser31, His37 and Trp41 residues, (b) top view of the M2 protein channel, and (c) the two inhibitors, where the distance scale *L* was used for the density plot shown in Fig. 2. *L* = 14 and 50 Å denote coordinates of the ends of the N- and C-terminals, respectively.

2440 molecules of FLEXSPC water [37]. The simulated systems were neutralized by counterions and the solvated box dimensions were set to 60 Å × 60 Å × 70 Å.

The simulations were carried out using the GROMACS 3.2.1 package [38] with the GROMACS force field [39], and Dundee PRODRG2 [40] was used to generate the inhibitor's topology file. The whole structure was minimized by the steepest descent algorithm. In the next stage, the system was equilibrated for 0.5 ns with position restraints on the protein atoms to improve the packing of lipids around the protein, following by an 8 ns MD simulation. The structural coordinates from simulations were saved every 0.5 ps for analysis.

For all simulations, the periodic boundary condition with the NPT ensemble was employed. The LINCS algorithm [41] was applied to constrain bond lengths and angles involving hydrogen atoms, and a 2 fs time step was used. Systems were coupled separately to a Berendsen temperature bath [42] at 310 K, using a coupling constant $\tau_T = 0.1$ ps. The pressure of 1 bar was kept constant by semi-isotropic coupling of the system to a Berendsen pressure bath [42]. Long-range interactions were involved within a twin-range cutoff: 1.2 nm for van der Waals interactions, and 1.2 nm for electrostatic interactions computed using the Particle Mesh Ewald (PME) algorithm [43]. The analysis phase was from 4 ns to 8 ns, in which the convergences of energies, temperature, pressure, and global root mean square displacement (RMSD) were used to verify the equilibrium of the systems.

3. Results and discussion

3.1. Water transport through the M2 channel

Water transport was monitored in terms of water density across the M2 channel where $L = 14$ Å starts from the N-terminal (see Fig. 1). To understand the movement of the inhibitors and their locations relative to the histidine gate and pore lining Ala30, distributions of inhibitors as well as the average coordination of the protonated and non-protonated histidine and four alanines were also plotted in Fig. 2.

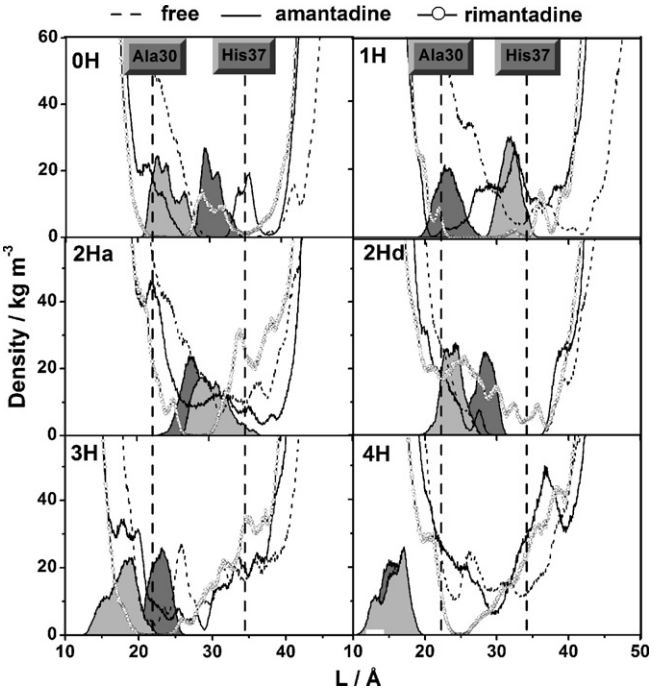

Fig. 2. Water density plots for free M2 and its inhibitor complexes. Water density along the M2 channel (see Fig. 1 for the definition of the distance L) for free M2 and its complexes with amantadine and rimantadine in the 6 protonation states (0H, 1H, 2Ha, 2Hd, 3H, and 4H), where the filled areas (dark gray for amantadine and light gray for rimantadine) represent distributions of the inhibitor's coordinates along the channel and the vertical dashed lines indicate average positions of the four alanines (Ala30) and four histidines (His37).

Without the inhibitor, water density for the 0H state (Fig. 2, top panel, dashed line) decreases exponentially and approached zero at ~28 Å, then starting to increase at ~40 Å. This character, which is also true for 2Hd state, indicates a solvent free-region where water cannot penetrate through the channel. In conclusion, among the six states of M2 in free form, water transport was observed to take place in the 1H, 2Ha, 3H and 4H states. A discrepancy was found in comparison with the previous MD results for free M2 channels [18], in which water was also detected to move through the channel in the 2Hd state. For clarification, consider the fact that water transport can take place in the M2 channel only at pH < 7 [23,44–47], for high protonation states of the histidine gate. It was recently found using NMR measurements that the 2Hd states yield a pH of 7.3 [19]. This datum supports our finding clearly.

For the M2-inhibitor complexes, non-zero water densities were noticeably found in the 2Ha, 3H and 4H states of the amantadine complexes and slightly detected in the 2Hd state of the rimantadine system (Fig. 2). This leads to the clear conclusion that water was better inhibited by rimantadine than amantadine. This fact was strongly supported by the experimental evidence in which the IC_{50} value of 0.98 ± 0.10 μg ml^{-1} for M2-rimantadine is over 10-fold lower than that of 13.8 ± 1.7 μg ml^{-1} for the M2-amantadine complexes [48]. In addition, the observed decrease of water density in the 3H state of the amantadine complex agrees well with that reported using MS-EVB study [34].

In terms of inhibitor mobility in the M2 channel, it was shown by the distribution plot of the inhibitors (filled areas in Fig. 2) to be localized at specific binding sites of the M2 channel. It can be also seen from the plots that distance from the pore (N-terminal) of the channel to the inhibitor's center of mass (D_{dept}) depends directly on the protonation state of the protein, *i.e.*, the inhibitors were observed, somehow, to be located deeper in the channels of lower protonation states. This fact can be described by an increase of the

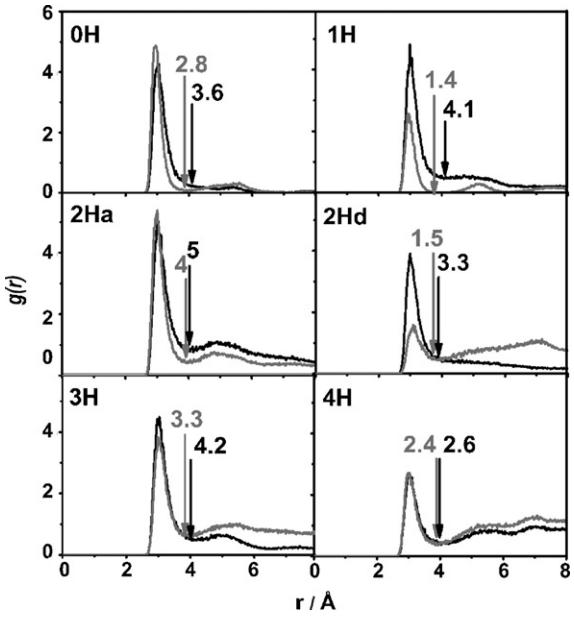

Fig. 3. Radial distribution functions, $g(r)$. Plots of $g(r)$ from nitrogen atoms of amantadine (black) and rimantadine (gray) to oxygen atoms of water. First-shell coordination numbers integrated up to the first minimum (marked by an arrow) are indicated.

repulsive interaction due to an increase of positive charge on the histidine gates of the higher protonation states. However, no relation can be inferred regarding the D_{dept} values of the two inhibitors. Amantadine can approach closer to the histidine gate for the 0H and 2Hd states, while rimantadine is closer for the 1H and 2Ha states (the average position of histidines is shown by vertical dashed lines in Fig. 2). Excluding the 4H system, where the inhibitors were found to locate almost above the opening pore, interest is focused on the 2Ha, 2Hd and 3H states, in which non-zero water densities were found beyond the distribution of the inhibitor's coordinates. In other words, water was observed to penetrate through the inhibitors. An answer to this fact relates directly to the inhibitor–solvent and inhibitor–protein interactions, which are described in the next sections.

3.2. Inhibitor–solvent interaction

The inhibitor–solvent interaction was monitored in terms of atom-atom radial distribution functions (RDFs), expressed as $g_{ij}(r)$, the probability of finding a particle of type j in a sphere of radius, r, around a particle of type i. Fig. 3 shows RDFs centered on the N atoms of inhibitor side chains and the O atoms of water. The corresponding first-shell coordination numbers integrated up to the first minimum are also indicated. All plots show a first sharp peak at ~3 Å, indicating that side chains of both inhibitors were firmly solvated. No significant difference was found in terms of the peak position. A clear conclusion can be drawn regarding the first shell coordination numbers. Excluding the 4H state, the number of water molecules around the amantadine side chain is significantly higher than for rimantadine, *i.e.*, the RDF data provide clear evidence that amantadine is solvated by more water molecules than rimantadine.

3.3. Mobility of the inhibitor in the M2 channel

In addition to determining the depth to which inhibitors can penetrate into the channel (Section 3.1 and filled areas shown in Fig. 2), we also determine their locations in the lateral x and y dimensions. In Fig. 4, the center of mass of the adamatane group (excluding the side chains) is projected onto the square formed by the four C_α atoms of the histidine tetrad, leading to the following conclusions: (i) all peaks are sharp and pronounced, located away

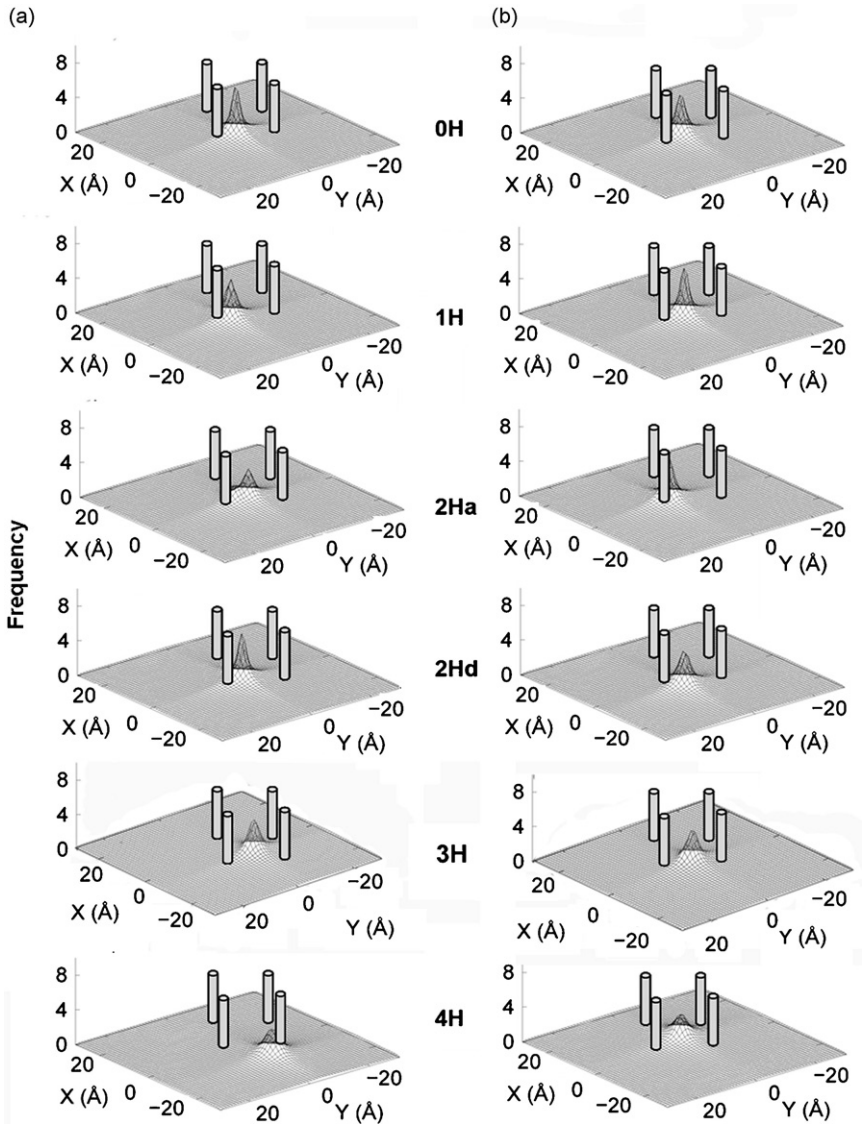

Fig. 4. Density of M2 inhibitor center of mass. Frequency (vertical axis) of center of mass locations from the twelve simulated systems of (a) amantadine and (b) rimantadine projected onto the square (*xy*-plane) formed by the four C_α atoms (represented by cylindrical tubes) of the histidine tetrad.

from the center of the *xy*-plane. This indicates localization of the inhibitors close to the residues of M2. This finding agrees well with the inhibitor–protein interaction data described in Section 3.4. (ii) The plots for rimantadine are slightly broader than those for amantadine. This confirms the N–O RDFs shown in Fig. 3, where amantadine side chain was found to bind more strongly to the solvated water molecules compared with rimantadine, thus allowing the solvated rimantadine to move more freely without carrying any nearest-neighbor water molecules.

3.4. Inhibitor binding site in the M2 channel

The number and percentage of hydrogen bonds between inhibitor molecules and the protein were investigated separately for the 4 units of the M2 tetramer. The bonds are defined by the default of the GROMACS program, *i.e.*, proton donor–acceptor distance $\leq$3.5 Å and donor–H–acceptor bond angle $\geq$120°. The results are shown in Fig. 5.

Again, the 4H state was not taken into consideration. As shown in Fig. 5, the plots lead to the following conclusions: (i) the inhibitors were found to form hydrogen bonds with four binding sites, located at the opening pore residues (Lue26, Ala30 and Ser31) and the histidine gate (His37). Interestingly, Leu26 Ala30 and Ser31 are the three residues previously associated with resistance to amantadine [12,23,49,50]. (ii) As expected, the inhibitors were observed to bind very weakly to the channel due to their allosteric hindrance. The strongest hydrogen bond is formed between the imidazole ring of His37 and the ammonium group of the inhibitor in the 0H-amantadine and 1H-rimantadine complexes, with ~55% occupation. (iii) More hydrogen bonds and a higher percentage occupation were formed in the less protonated complexes, 0H and 1H, than in the more protonated complexes, 2Ha, 2Hd and 3H. This is due to the effect of repulsion between the $-NH_3^+$ groups of inhibitors and the positively charged imidazole ring of histidine in the more protonated systems, which contained a larger amount of protonated His37. The observed data are directly related to the distance from the pore (N-terminal) of the channel to the inhibitor's center of mass, D_{dept}, as shown in Fig. 2. (iv) An answer to the previously mentioned question of why water was better inhibited by rimantadine than amantadine is indicated by very weak hydrogen bonding in the 2Ha and 3H states (Fig. 5). For 2Ha state, rimantadine was detected to be localized slightly closer to histidine gate compared with amantadine (see distributions of the inhibitors in Fig. 2) and can facilitate the orientation of His37 to close the channel. The influence of the inhibitors on the His37 orientation can be obviously exhibited by the protein-amantadine (0H state) and protein-rimantadine (1H state) configurations as mentioned in (ii). This finding agrees well with the mechanism proposed by Pinto et al. based on results from the cysteine scanning mutagenesis technique [31,47] which stated that inhibitor binding to the His37 side chain can interfere with the histidine facilitation of proton conductance. The proposed mechanism was also supported by the NMR results published recently by Hu et al. [33].

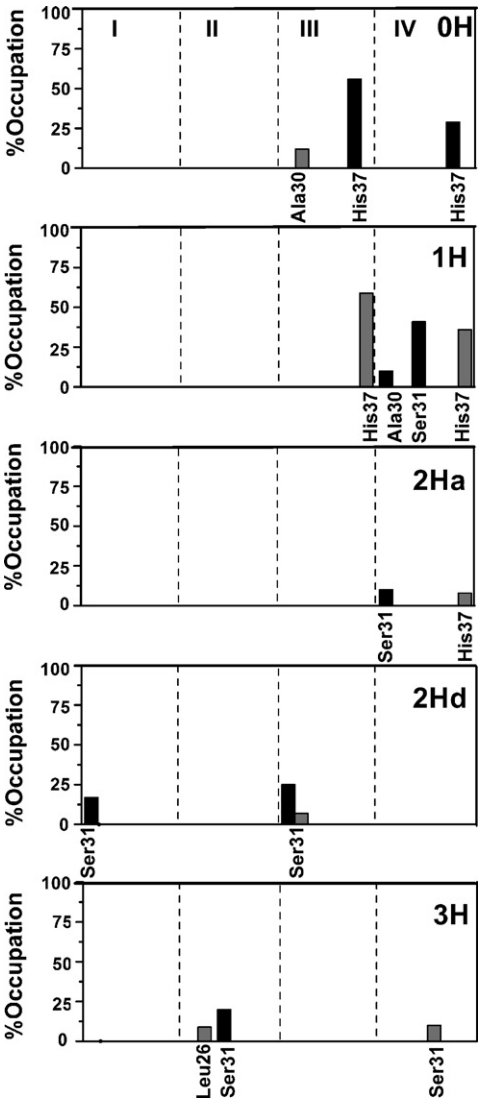

Fig. 5. Hydrogen bond occupations between M2 residues and inhibitors. The hydrogen bond occupation between M2 residues and the inhibitors amantadine (black) and rimantadine (gray) for the ten simulated systems, where I–IV denote the four units of the M2 protein tetrad.

Besides the above mechanism, an alternative mechanism was indicated by the interaction between inhibitors and three opening pore residues, Lue26, Ala30 and Ser31, which are located approximately 5 Å from the N-terminal (see also Fig. 1a). Binding to either Ala30 or Ser31 was detected in almost all states of the drug-blocked complexes while the binding of Leu26 was only observed in 3H-rimantadine system as shown in Fig. 5. This mechanism agrees well with a hypothesis that the inhibitor acts as a blocker by interacting with the mouth of the M2 pore [25,27]. However, referring to the lower inhibition of amantadine than rimantadine in the 2Ha state (see Fig. 2), this inhibition mechanism could have a lower efficiency compared with that where inhibitor binds with the histidine gate. A clear picture of the two mechanisms and detailed descriptions are given again in Fig. 7 and Section 3.5, respectively.

3.5. Orientation of inhibitor in M2 channel

The orientation of the inhibitor embedded in the channel was visualized in terms of the distribution of an angle θ (see inset of Fig. 6). The angle was defined by two vectors, of which one points along the C–X bond, where X denotes an N atom for amantadine and a C1 atom for rimantadine (see Fig. 1), and the other lies parallel to the channel and points from the N- to the C-terminal of the M2 protein. The second vector is parallel to the line connecting between the center of the two squares formed by the C_α atoms of the 4 histidines (His37) and the 4 tryptophans (Trp41), respectively, *i.e.*, it lies parallel to the channel and points from the N- to the C-terminal of the M2 protein. For simplicity, the second vector was termed the channel axis. The results are shown in Fig. 6. By definition, this means that the inhibitor points its side chain along

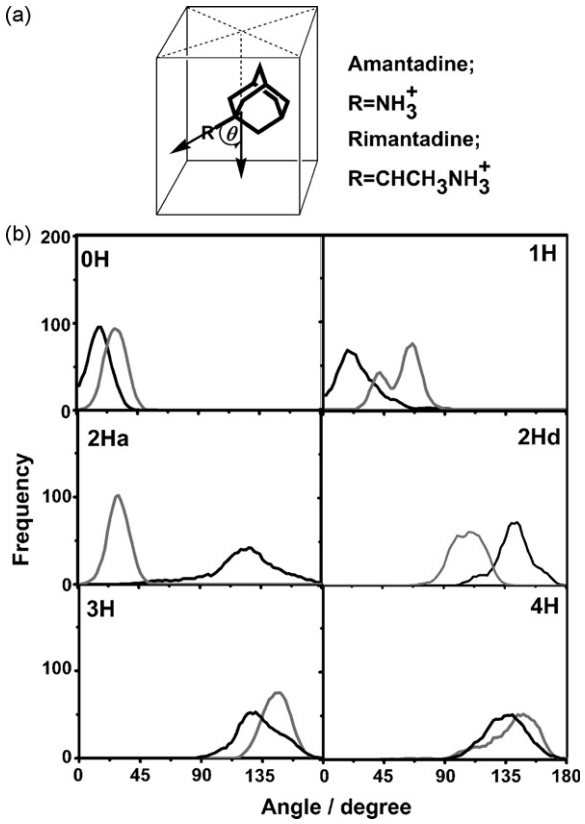

Fig. 6. Orientation of the inhibitors. (a) Distribution of the angle θ, defined in (b) by 2 vectors, of which one points along the C–X bond (where X = N and C for amantadine and rimantadine, respectively) and the other points parallel to the M2 channel from the N- to the C-terminal (see text for details).

the channel in the direction to the C- or N-terminal for $\theta = 0^\circ$ or 180°, respectively.

The plots show very clearly that the two inhibitors in the 0H and 1H states were found to point their side chains in the direction toward the C terminal, and maxima of the peaks appeared at $\theta < 90^\circ$. At higher protonation states, an increase of partial charges on the His37 groups leads to a reorientation of the inhibitors as can be seen of both inhibitors in 3H state. As shown in Fig. 6, the transition from $\theta < 90^\circ$ to $\theta > 90^\circ$ was observed in the 2Ha-amantadine and 2Hd-rimantadine. The change of the rimantadine's orientation leads us to understand that symmetrical 2Hd diprotonation generates a stronger repulsion of the inhibitor side chain than the asymmetrical 2Ha state. In addition, an easier reorientation of amantadine (at the 2Ha state) than rimantadine (at the 2Hd state), could be due to the lower steric effect of its $-NH_3^+$ side chain in comparison with $-CHCH_3NH_3^+$ of rimantadine, especially when were embedded in a limited space in the M2 channel.

To clearly monitor the above observations in detail, the positions and orientations of the inhibitors were carefully determined from Figs. 2 and 4–6. They were sketched relative to the positions of the four binding residues of the M2 protein, Lue26, Ala30, Ser31 and His37. The results are given in Fig. 7. Let us consider amantadine in the 0H state as an example. It was found in Fig. 2 to be located between Ser31 and His37 at $L \sim 16$ Å from the mouth of the pore and ~5 Å above the His37. Its position (Fig. 4) is not at the center of the M2-channel, *i.e.*, not at the center of the *xy* plane defined in Section 3.3. It was also shown in Fig. 5 to form hydrogen bonds with His37. In addition, its side chain was observed in Fig. 6 to preferentially point to the N terminal with

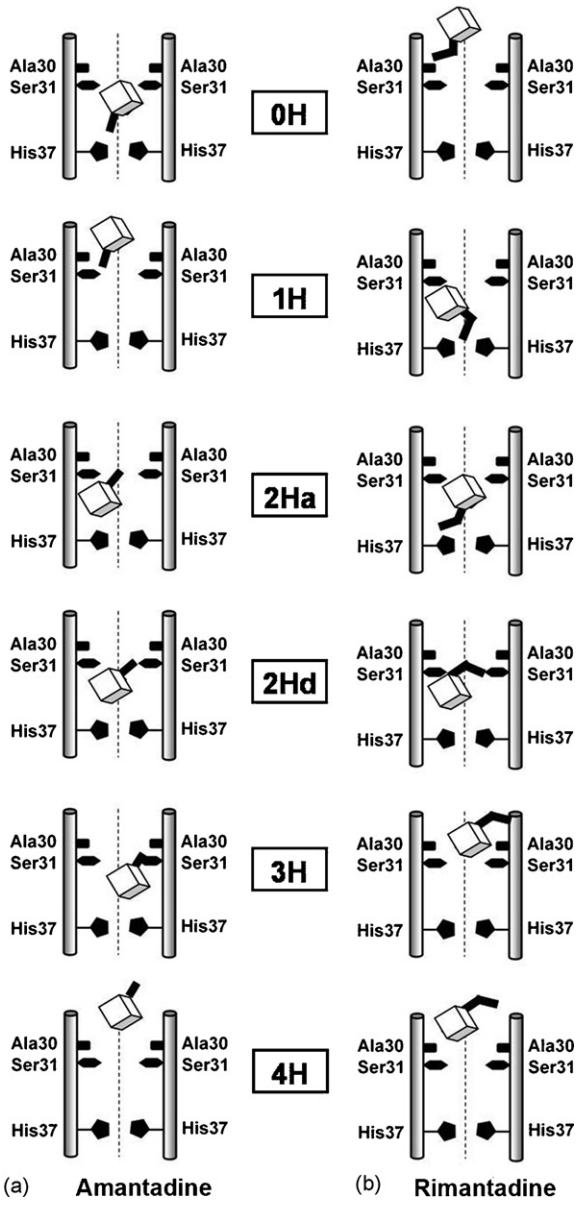

Fig. 7. Position and orientation of inhibitors in M2 channel. Sketches showing the position and orientation of (a) amantadine and (b) rimantadine as summarized from Figs. 2 and 4–6 (see text for details).

$\theta = 20^\circ$, according to the maximum of the distribution plot in Fig. 6. With the same procedures, schematic representations of the position and orientation of the two inhibitors in the M2 channel are portrayed in Fig. 7.

Besides a clear understanding of the preferential position and orientation of the two inhibitors for the different protonation states of the M2-protein channel, the two mechanisms of action where drugs bind to the opening pore and the His37 gate were clearly displayed (see discussion in the last part of Section 3.4).

4. Conclusions

We have performed MD simulations on the six possible His37 protonation states of the proton-selective M2 tetrameric channel in free form and complexed with two inhibitors, amantadine and rimantadine, in a fully hydrated lipid bilayer. The results indicate that water density in the channel was noticeably reduced by the

inhibitors, especially in the M2-rimantadine complex. The observed data agrees very well with the experimental IC_{50}. In term of drug-target binding, the simulated results was supported by the two previously proposed mechanisms of action of the inhibitors that drug molecules are likely to bind within either the inner cavity or the external mouth of the channels. The two corresponding binding sites of the inhibitors in the M2 channel are near the histidine gate (His37) and the opening pore residues (Leu26, Ala30 and Ser31). In both important regions, the simulated data imply a mechanism by which the inhibitor localizes and interacts weakly with the side chains of the binding site residues. This will, consequently facilitate the orientation of these side chains to lie almost perpendicular to the inner surface of the channel. The proposed mechanisms provide a clear description toward an ultimate goal of this study, to explain how drugs inhibit proton transport in the M2 protein channel.

Acknowledgements

This work was supported by the Thailand Research Fund. The authors would like to thank the Post-Doctoral Program from the Commission on Higher Education. The Computer Center for Advanced Research and the Computational Chemistry Unit Cell, Faculty of Science, Chulalongkorn University provided research facilities, software packages and computing time. We thank National Nanotechnology Center (NANOTEC), NSTDA, Thailand for Dicovery Studio version 1.7.

References

[1] N.J. Cox, K. Subbarao, Global epidemiology of influenza: past and present, Annu. Rev. Med. 51 (2000) 407–421.
[2] A.H. Reid, J.K. Taubenberger, The origin of the 1918 pandemic influenza virus: a continuing enigma, J. Gen. Virol. 84 (2003) 2285–2292.
[3] R.G. Webster, E.A. Govorkova, H5N1 influenza—continuing evolution and spread, New Engl. J. Med. 355 (2006) 2174–2177.
[4] M.D.d. Jong, T.T. Hien, Avian influenza A (H5N1), J. Clin. Virol. 35 (2006) 2–13.
[5] R.A. Lamb, S.L. Zebedee, C.D. Richardson, Influenza virus M2 protein is an integral membrane protein expressed on the infected-cell surface, Cell 40 (1985) 627–633.
[6] L.J. Holsinger, R.A. Lamb, Influenza virus M2 integral membrane protein is a homotetramer stabilized by formation of disulfide bonds, Virology 183 (1991) 32–43.
[7] R.J. Sugrue, A.J. Hay, Structural characteristics of the M2 protein of influenza A viruses: evidence that it forms a tetrameric channel, Virology 180 (1991) 617–624.
[8] T. Sakaguchi, Q. Tu, L.H. Pinto, R.A. Lamb, The active oligomeric state of the minimalistic influenza virus M2 ion channel is a tetramer, Proc. Natl. Acad. Sci. U.S.A. 94 (1997) 5000–5005.
[9] K.C. Duff, R.H. Ashley, The transmembrane domain of influenza A M2 protein forms amantadine-sensitive proton channels in planar lipid bilayers, Virology 190 (1992) 485–489.
[10] A. Kukol, P.D. Adams, L.M. Rice, A.T. Brunger, I.T. Arkin, Experimentally based orientational refinement of membrane protein models: a structure for the influenza A M2 H+ channel, J. Mol. Biol. 286 (1999) 951–962.
[11] J. Wang, S. Kim, F. Kovacs, T.A. Cross, Structure of the transmembrane region of the M2 protein H+ channel, Protein Sci. 10 (2001) 2241–2250.
[12] K. Nishimura, S. Kims, L. Zhang, T.A. Cross, The closed state of a H+ channel helical bundle combining precise orientational and distance restraints from solid state NMR, Biochemistry 41 (2002) 13170–13177.
[13] C. Tian, P.F. Gao, L.H. Pinto, R.A. Lamb, T.A. Cross, Initial structural and dynamic characterization of the M2 protein transmembrane and amphipathic helices in lipid bilayers, Protein Sci. 12 (2003) 2597–2605.
[14] A. Okada, T. Miura, H. Takeuchi, Protonation of histidine and histidine–tryptophan interaction in the activation of the M2 ion channel from influenza a virus, Biochemistry 40 (2001) 6053–6060.
[15] M.F. Mesleh, G. Veglia, T.M. DeSilva, F.M. Marassi, S.J. Opella, Dipolar waves as NMR maps of protein structure, J. Am. Chem. Soc. 124 (2002) 4206–4207.
[16] L.H. Pinto, G.R. Dieckmann, C.S. Gandhi, M.A. Shaughnessy, C.G. Papworth, J. Braman, J.D. Lear, R.A. Lamb, W.F. DeGrado, A functionally defined model for the M2 proton channel of influenza A virus suggests a mechanism for its ion selectivity, Proc. Natl. Acad. Sci. U.S.A. 94 (1997) 11301–11306.
[17] L.R. Forrest, A. Kukol, I.T. Arkin, D.P. Tieleman, M.S.P. Sansom, Exploring models of the influenza A M2 channel: MD simulations in a phospholipid bilayer, Biophys. J. 78 (2000) 55–69.
[18] I. Kass, I.T. Arkin, How pH opens a H+ channel: the gating mechanism of influenza A M2, Structure 13 (2005) 1789–1798.
[19] J. Hu, R. Fu, K. Nishimura, L. Zhang, H.-X. Zhou, D.D. Busath, V. Vijayvergiya, T.A. Cross, Histidines, heart of the hydrogen ion channel from influenza A virus: toward an understanding of conductance and proton selectivity, PNAS 103 (2006) 6865–6870.
[20] M.S.P. Sansom, I.D. Kerr, G.R. Smith, H.S. Son, The influenza A virus M2 channel: a molecular modeling and simulation study, Virology 233 (1997) 163–173.
[21] J.S. Oxford, A. Galbraith, Antiviral activity of amantadine: a review of laboratory and clinical data, Pharmacol. Ther. 11 (1980) 181–262.
[22] R. Dolin, R.C. Reichman, H.P. Madore, R. Maynard, P.N. Linton, J. Webber-Jones, A controlled trial of amantadine and rimantadine in the prophylaxis of influenza A infection, New Engl. J. Med. 307 (1982) 580–584.
[23] L.H. Pinto, L.J. Holsinger, R.A. Lamb, Influenza virus M2 protein has ion channel activity, Cell 69 (1992) 517–528.
[24] R.J. Sugrue, A. Hay, Structural characteristics of the M2 protein of influenza A viruses: evidence that it forms a tetrameric channel, J. Virol. 180 (1991) 617–624.
[25] A.J. Hay, The action of adamantanamines against influenza A viruses: inhibition of the M2 ion channel protein, Semin. Virol. 3 (1992) 21–30.
[26] R.A. Lamb, L.J. Holsinger, L.H. Pinto, in: E. Wimmer (Ed.), Receptor-mediated virus entry into cells, Cold Spring Harbor Laboratory Press, New York, 1994, pp. 303–321.
[27] M.S.P. Sansom, I.D. Kerr, Influenza virus M2 protein: a molecular modelling study of the ion channel, Prot. Eng. 6 (1993) 65–74.
[28] K.C. Duff, P.J. Gilchrist, A.M. Saxena, J.P. Bradshaw, Neutron diffraction reveals the site of amantadine blockade in the influenza A M2 ion channel, Virology 202 (1994) 287–293.
[29] C.S. Gandhi, K. Shuck, J.D. Lear, G.R. Dieckmann, W.F. DeGrado, R.A. Lamb, L.H. Pinto, Cu(II) inhibition of the proton translocation machinery of the influenza A virus M2 protein, J. Biol. Chem. 274 (1999) 5474–5482.
[30] C. Wang, K. Takeuchi, L.H. Pinto, R.A. Lamb, Ion channel activity of influenza A virus M2 protein: characterization of the amantadine block, J. Virol. 67 (1993) 5585–5594.
[31] L.H. Pinto, R.A. Lamb, Controlling influenza virus replication by inhibiting its proton channel, Mol. BioSyst. 3 (2007) 18–23.
[32] A. Kolocouris, R.K. Hansen, R.W. Broadhurst, Interaction between an amantadine analogue and the transmembrane portion of the influenza A M2 protein in liposomes probed by 1H NMR spectroscopy of the ligand, J. Med. Chem. 47 (2004) 4975–4978.
[33] J. Hu, T. Asbury, S. Achuthan, C. Li, R. Bertram, J.R. Quine, R. Fu, T.A. Cross, Backbone structure of the amantadine-blocked trans-membrane domain M2 proton channel from influenza A virus, Biophys. J. 92 (2007) 4335–4343.
[34] H. Chen, Y. Wu, G.A. Voth, Proton transport behavior through the influenza A M2 channel: insights from molecular simulation, Biophys. J. 93 (2007) 3470–3479.
[35] G.M. Morris, D.S. Goodsell, R.S. Halliday, R. Huey, W.E. Hart, R.K. Belew, A.J. Olson, Automated docking using a lamarckian genetic algorithm and empirical binding free energy function, J. Comp. Chem. 19 (1998) 1639–1662.
[36] L.R. Forrest, D.P. Tieleman, M.S.P. Sansom, Defining the transmembrane helix of M2 protein from influenza A by molecular dynamics simulations in a lipid bilayer, Biophys. J. 76 (1999) 1886–1896.
[37] H.J.C. Berendsen, J.P.M. Postma, W.F. van Gunsteren, J. Hermans, Intermolecular Forces, Reidel, Dordrecht, The Netherlands, 1981.
[38] E. Lindahl, B. Hess, D. van der Spoel, GROMACS 3.0: a package for molecular simulation and trajectory analysis, J. Mol. Model. 7 (2001) 306–317.
[39] J. Hermans, H.J.C. Berendsen, W.F. van Gunsteren, J.P.M. Postma, A consistent empirical potential for water–protein interactions, Biopolymers 23 (1984) 1513–1518.
[40] D.M. van Aalten, R. Bywater, J.B. Findlay, M. Hendlich, R.W. Hooft, G. Vriend, PRODRG, a program for generating molecular topologies and unique molecular descriptors from coordinates of small molecules, J. Comput. Aided Mol. Des. 10 (1996) 255–262.
[41] B. Hess, H. Bekker, H.J.C. Berendsen, J.G.E.M. Fraaije, LINCS: a linear constraint solver for molecular simulations, J. Comp. Chem. 18 (1997) 1463–1472.
[42] H.J.C. Berendsen, J.P.M. Postma, W.F. van Gunsteren, A. DiNola, J.R. Haak, Molecular dynamics with coupling to an external bath, J. Chem. Phys. 81 (1984) 3684–3690.
[43] T. Darden, D. York, L. Pedersen, Particle mesh Ewald: an N–log(N) method for Ewald sums in large systems, J. Chem. Phys. 98 (1993) 10089–10092.
[44] I.V. Chizhmakov, F.M. Geraghty, D.C. Ogden, A. Hayhurst, M. Antoniou, A.J. Hay, Selective proton permeability and pH regulation of the influenza virus M2 channel expressed in mouse erythroleukaemia cells, J. Physiol. (Lond.) 494 (1996) 329–336.
[45] I.V. Chizhmakov, D.C. Ogden, F.M. Geraghty, A. Hayhurst, A. Skinner, T. Betakova, A.J. Hay, Differences in conductance of M2 proton channels of two influenza viruses at low and high pH, J. Physiol. (Lond.) 546 (2003) 427–438.
[46] C. Wang, R.A. Lamb, L.H. Pinto, Activation of the M2 ion channel of influenza virus: a role for the transmembrane domain histidine residue, Biophys. J. 69 (1995) 1363–1371.
[47] J.A. Mould, J.E. Drury, S.M. Frings, U.B. Kaupp, A. Pekosz, R.A. Lamb, L.H. Pinto, Permeation and activation of the M2 ion channel of influenza A virus, J. Biol. Chem. 275 (2000) 31038–31050.
[48] J.M. Kelly, M.A. Miles, A.C. Skinner, The anti-influenza virus drug rimantadine has trypanocidal activity, Antimicrob. Agents Chemother. 43 (1999) 985–987.
[49] J.A. Englund, Antiviral therapy of influenza, Semin. Pediatr. Infect. Dis. 13 (2002) 120–128.
[50] A.J. Hay, A.J. Wolstenholme, J.J. Skehel, M.H. Smith, The molecular basis of the specific anti-influenza action of amantadine, EMBO J. 4 (1985) 3021–3024.